Indian Journal of Chemical Technology
Vol. 31, January 2024, pp. 57-69
DOI: 10.56042/ijct.v31i1.3263

# Impact of Cattaneo-Christov heat flux on mixed convection flow of a ternary hybrid (Cu-$Al_2O_3$-$TiO_2$/$H_2O$) nanofluid over an elongated sheet: A comparative analysis

K. Madiha Takreem & P. V. Satya Narayana*

Department of Mathematics, School of Advanced Sciences, Vellore Institute of Technology, Vellore 632 014, Tamil Nadu, India

*E-mail: pvsatya8@yahoo.co.in

*Received 28 June 2023; accepted 12 December 2023*

The transfer of heat is an ineluctable part of science and engineering. The ternary hybrid nanofluid with its refined thermal properties exhibits superior heat transport capacity compared to hybrid nanofluids. Bearing in mind the extensive applications of this advanced fluid, the current research article deliberately investigates the impact of Cattaneo-Christov heat flux on the flow of a ternary hybrid nanofluid over an elongated sheet in the existence of thermal radiation. The proposed model is formulated by considering a base fluid of water dispersed with three distinct nanoparticles, $Cu$, $Al_2O_3$, and $TiO_2$. An application of the similarity transformation is made to change the controlling equations of the flow in dimensionless form. A numerical solution of the resulting equations is obtained by utilizing the bvp4c algorithm in MATLAB software. The results revealed that amplification in the values of the mixed convection parameter enhances the velocity profile of the ternary hybrid nanofluid and there is an advanced thermal transmission rate under the sway of Cattaneo-Christov thermal theory. It is further inferred from the current study that with varying volume fractions, trihybrid nanofluid demonstrates approximately 1.82-5.46% greater heat transfer than $TiO_2$ / $H_2O$ nanofluid and exhibits a stupendous thermal transmission rate over hybrid nanofluid and nanofluid.

**Keywords:** Cattaneo-Christov (C-C) thermal flux, Mixed convection, Stretching sheet, Ternary hybrid nanofluid, Thermal radiation

## Introduction

Recent years have seen a significant increase in research on heat transfer up-gradation in industrial and production fields. This is attributed to the fact that the rate at which the heat is conducted determines the efficacy of most of the electronics, power generators, heat exchangers, etc. In order to acquire substantial enhancement in thermal transfusion rate, Choi and Eastman[1] proposed the notion of nanofluids, which are made by dispersing nanoparticles into conventional fluids. Nanofluids have proven to be beneficial in multiple fields of industrial and engineering applications, such as microelectronics, fuel chambers, pharmaceutical processes, nuclear reactors, and temperature reduction[2]. Though the nanofluids seem to intensify the thermal conductivity (TC), industries need fluids which has a superior rate of heat transfer (RHT) compared with regular nanofluid. Hybrid nanofluids are fabricated by diffusion of two or more nanoparticles in the fluid base. As a result of their exceptional TC, hybrid nanofluids have found numerous applications in various fields such as in tinning wires, space devices, crude oil extraction, welding, atomic reactors, the brake fluid of automobiles, etc. There are several factors contributing to the effective TC of hybrid nanofluids, such as how it is prepared, their size, shape factor, rate of dispersion of nanoparticles, surfactants, temperature, volume concentration, etc. By varying the temperature, Aparna *et al.*[3] experimentally evaluated the TC of aqueous $Al_2O_3 - Ag/ H_2O$. As per the conclusion drawn from the study, a high temperature resulted in enlarged TC for the hybrid nanofluid. The leverage of nanoparticle size and structure on the hydrothermal behavior of plate evaporators by utilizing different hybrid combinations was explored by Bhattad and Sarkar[4]. They concluded that the functioning of the plate exchanger is robustly affected by the shape of the nanoparticles and the nanoparticles shaped like bricks are the most effective in heat transfer. Using $GO - MoS_2 / H_2O$ hybrid nanofluid, Kulkarni[5] evaluated

the consequence of slip effect and thermal transfer features past a porous disk and inferred that the thermal transmission rate augments with enhancing nanoparticle sphericity.

Recent research about the nanofluids made by dispersion of three different nanoparticles has stimulated the inquisitiveness of researchers due to their strengthened heat transfer potentiality. This nanofluid, also known as tri-hybrid or ternary hybrid nanofluid, has an exceptional TC in comparison with regular and hybrid nanofluids. This was proved theoretically by Manjunatha *et al*.[6] who considered the $Al_2O_3 - TiO_2 - SiO_2 / H_2O$ trihybrid combination to ascertain the heat transmission features. Dezfulizadeh *et al*.[7] investigated $Cu - SiO_2 - MWCNT / H_2O$ ternary hybrid nanofluid with respect to its TC. In addition to evaluating its dynamic viscosity, they found the tri-hybrid nanofluid flaunts finer TC and enhanced viscosity over mono nanofluids and hybrid nanofluids. The ternary hybrid nanofluid $CuO - MgO - TiO_2 / H_2O$ was explored by Mousavi *et al*.[8] by varying the nanoparticle mixture ratio and temperature. They concluded that compared to purified $H_2O$, the tri-hybrid nanofluid in a combinative 60:30:10 ratio has the greatest TC which possessed an improvement by 78.6% for a volume fraction of 0.1% at 50℃. Their enriched heat transmission capability makes the THNF an ideal choice for applications in various sectors such as coolant in radiators[9], in the photovoltaic thermal system[10], evaporative coolers[11], etc. Few of the tectonic works done on heat transfer analysis involving ternary nanofluid can be referred[12-16].

Combined forced and natural convection, also called mixed convection, is a mechanism in which both free and forced convection work together to transfer thermal energy. Mixed convection problems past a stretching sheet have captivated the interest of researchers over the past few decades. This is due to their broad list of applications in numerous fields such as nuclear reactors, electronics, petroleum reservoirs, chemical reactors, solar receivers, etc. El-Shorbagy *et al*.[17] analyzed the mixed convective flow of $Al_2O_3 / H_2O$ nanofluid in a trapezoid shaped channel embedded in a porous media. They inspected the impact of thermal transfer on parameters such as Richardson number and Darcy number and concluded that a drop in the values of Richarson number accelerates the heat transfer rate, whereas heat transfer is affected differently by Darcy number at every porous height. A numerical investigation on the mixed convection flow of $Al_2O_3 / H_2O$ nanofluid past a circular cylinder embedded in a porous media was studied by Al-Farhany and Abdulsahib[18] and detected that elevating the values of Darcy number and volume fractions results in an increase in the values of Nusselt number. Waini *et al*.[19] examined the steady mixed convective flow of $Al_2O_3 - Cu / H_2O$ hybrid nanofluid over an impermeable vertical surface and deduced that a decline in the mixed convective parameter degrades the velocity sketch of the hybrid nanofluid. There are also similar studies concerning free cum forced convection of hybrid nanofluid in[20-25].

The transfer of energy(heat) as electromagnetic waves is referred to as "thermal radiation". Radiative heat transfer in flow problems has profound impacts in the designing of propulsion devices, thermal systems, solar power plants, in the polymer industry, etc. The impact of radiation heat transfer in a natural convective flow of $Al_2O_3 / H_2O$ nanofluid within a diagonal rectangular enclosure was analyzed by Pordanjani *et al*.[26]. Their study claimed that the rate at which the heat is transferred within the enclosure can be compounded by enhancing the values of radiation parameter. Reddy and Sreedevi[27] analyzed the contribution of thermal radiation to heat transmission characteristics of $SWCNT / H_2O$ nanofluid inside a square cavity and found that the heat transmission coefficient increases with accelerating values of the radiation parameter. A case study for estimating the thermal transport attributions of an unsteady MHD flow of a Casson nanofluid with the existence of radiation was carried out by Jamshed *et al*.[28]. The sway of thermal radiation on the unsteady 2-D flow of $MWCNT - Ag / H_2O$ hybrid nanofluid along an elongated sheet was addressed by Sreedevi *et al*.[29]. Escalation in temperature is observed with raising values of the radiation parameter and volume fraction of the nanoparticles. Wahid *et al*.[30] observed the same configuration of the temperature field in their investigation of the steady, mixed convective flow of a hybrid nanofluid over a flat vertical plate.

In general, heat transfer occurs when there exists a temperature gradient between two different materials or within the same one. The analysis of thermal transfer has been done by using Fourier's law of heat conduction for centuries. But this classical law has the disadvantage that initial disruptions propagate

throughout the entire process. Cattaneo cleared this issue by fusing the term of thermal relaxation in Fourier's law. Later, Christov proposed a derivative law of Cattaneo, and the resulting thermal flux model is designated as the Cattaneo-Christov (C-C) thermal flux model. Based on the C-C thermal theory, Reddy *et al.*[31] examined the thermal transport features of an MHD nanofluid flow passing through a whirling cylinder. Their study reported that the RHT strengthens with intensifying values of the thermal relaxation parameter. A comparative study between the thermal transport characteristics of distinct nanoparticles $Cu$ and $CuO$ in two distinct limitedly ionized fluids characterized by C-C theory was carried out by Abid *et al.*[32]. Considering the effect of thermal radiation and C-C heat flux, Azam[33] explored the two-dimensional magnetized flow of an incompressible Maxwell nanofluid. He noticed that boosting the magnetic parameter results in a declination of the RHT. The axisymmetric flow of $Cu-Al_2O_3/H_2O$ hybrid nanofluid past a stretching/shrinking sheet in a porous medium was investigated by Khan *et al.*[34]. By employing C-C thermal flux, they developed a new iterative technique to find a numerical solution to the proposed model[35-40] provides some recent descriptions of C-C thermal flux.

The ultimate intent of this study is to scrutinize the C-C influence on the mixed convective flow of a two-dimensional ternary hybrid nanofluid. An abundance of literature is available on a similar characterized flow of nanofluids and hybrid nanofluids, but no investigations have yet been conducted on ternary hybrid nanofluids. Thus, an attempt has been made to address this issue in this study. In this investigation, the following research inquiries are addressed:

- How does the presence of mixed convection influence the two-dimensional flow of ternary hybrid nanofluid over an elongated sheet?
- What is the consequence of C-C thermal theory on the thermal profile of the ternary hybrid nanofluid?
- Which type of nanofluid exhibits enhanced thermal transmission characteristics? Hybrid or Ternary?

## Mathematical Formulation

The assumptions underlying fluid flow are as follows

1. Two-dimensional flow
2. Steady flow
3. Stretching sheet
4. Trihybrid nanofluid $\left(Cu-Al_2O_3-TiO_2/H_2O\right)$
5. Cattaneo-Christov heat flux
6. Incompressible ternary hybrid nanofluid

Thus, based on the assumptions outlined above, the flow of incompressible, trihybrid nanofluid past an elongated sheet has been considered in a steady, two-dimensional flow. In this model, $U_{\tilde{w}}=c\tilde{x}$ represents the velocity at which the sheet stretches. The configuration is portrayed through a rectangular coordinate system as shown in Fig. 1. The trihybrid nanofluid is created by suspending $Cu, Al_2O_3$, and $TiO_2$ nanoparticles in water.

Given the aforesaid assumptions, the concerning PDE for the ternary nanofluid flow is modeled as follows[30]

$$\frac{\partial\tilde{u}}{\partial\tilde{x}}+\frac{\partial\tilde{v}}{\partial\tilde{y}}=0 \qquad \ldots (1)$$

$$\tilde{u}\frac{\partial\tilde{u}}{\partial\tilde{x}}+\tilde{v}\frac{\partial\tilde{u}}{\partial\tilde{y}}=\frac{\mu_{tnf}}{\rho_{tnf}}\frac{\partial^2\tilde{u}}{\partial\tilde{y}^2}+g_r\frac{\left(\rho\beta_T\right)_{tnf}}{\rho_{tnf}}\left(\tilde{T}-\tilde{T}_\infty\right) \qquad \ldots (2)$$

$$\tilde{u}\frac{\partial\tilde{T}}{\partial\tilde{x}}+\tilde{v}\frac{\partial\tilde{T}}{\partial\tilde{y}}=\frac{k_{tnf}}{(\rho c_p)_{tnf}}\frac{\partial^2\tilde{T}}{\partial\tilde{y}^2}+\frac{16\sigma^*\tilde{T}_\infty^3}{3k^*(\rho c_p)_{tnf}}\frac{\partial^2\tilde{T}}{\partial\tilde{y}^2} -\lambda_\tau\left\{\begin{array}{l}\left(\tilde{u}\frac{\partial\tilde{u}}{\partial\tilde{x}}+\tilde{v}\frac{\partial\tilde{u}}{\partial\tilde{y}}\right)\frac{\partial\tilde{T}}{\partial\tilde{x}}+\left(\tilde{u}\frac{\partial\tilde{v}}{\partial\tilde{x}}+\tilde{v}\frac{\partial\tilde{v}}{\partial\tilde{y}}\right)\\ \frac{\partial\tilde{T}}{\partial\tilde{y}}+\tilde{u}^2\frac{\partial^2\tilde{T}}{\partial\tilde{x}^2}+\tilde{v}^2\frac{\partial^2\tilde{T}}{\partial\tilde{y}^2}+2\tilde{u}\tilde{v}\frac{\partial^2\tilde{T}}{\partial\tilde{x}\partial\tilde{y}}\end{array}\right\} \qquad \ldots (3)$$

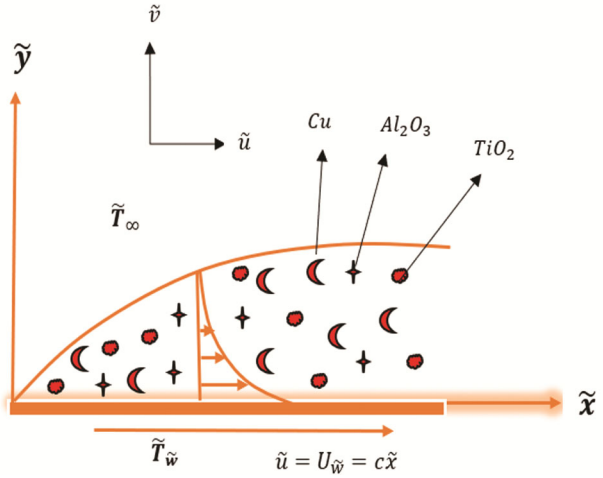


Fig. 1 — Configuration of the flow

Table 1 — Thermophysical characteristics of ternary hybrid nanofluid[6]

| Thermo-physical Property | Ternary Hybrid Nanofluid |
|---|---|
| Dynamic Viscosity | $\mu_{tnf} = \dfrac{\mu_f}{\left[(1-\phi_1)(1-\phi_2)(1-\phi_3)\right]^{10/4}}$ |
| Density | $\dfrac{\rho_{tnf}}{\rho_f} = (1-\phi_1)\left\{(1-\phi_2)\left[(1-\phi_3)+\phi_3\dfrac{\rho_3}{\rho_f}\right]+\phi_2\dfrac{\rho_2}{\rho_f}\right\}+\phi_1\dfrac{\rho_1}{\rho_f}$ |
| Heat Capacity | $\dfrac{(\rho c_P)_{tnf}}{(\rho c_P)_f} = (1-\phi_2)\left\{(1-\phi_3)\left[(1-\phi_1)+\phi_1\dfrac{(\rho c_P)_1}{(\rho c_P)_f}\right]+\phi_3\dfrac{(\rho c_P)_3}{(\rho c_P)_f}\right\}+\phi_2\dfrac{(\rho c_P)_2}{(\rho c_P)_f}$ |
| Thermal expansion Coefficient | $\dfrac{(\rho\beta_T)_{tnf}}{(\rho\beta_T)_f} = (1-\phi_2)\left\{(1-\phi_3)\left[(1-\phi_1)+\phi_1\dfrac{(\rho\beta_T)_1}{(\rho\beta_T)_f}\right]+\phi_3\dfrac{(\rho\beta_T)_3}{(\rho\beta_T)_f}\right\}+\phi_2\dfrac{(\rho\beta_T)_2}{(\rho\beta_T)_f}$ |
| Thermal conductivity | $\dfrac{k_{tnf}}{k_{hnf}} = \dfrac{k_1+2k_{hnf}-2\phi_1(k_{hnf}-k_1)}{k_1+2k_{hnf}+\phi_1(k_{hnf}-k_1)}$ |
| | Where $\dfrac{k_{hnf}}{k_{nf}} = \dfrac{k_2+2k_{nf}-2\phi_2(k_{nf}-k_2)}{k_2+2k_{nf}+\phi_2(k_{nf}-k_2)}$ and $\dfrac{k_{nf}}{k_f} = \dfrac{k_3+2k_f-2\phi_3(k_f-k_3)}{k_3+2k_f+\phi_3(k_f-k_3)}$ |

with the boundary constraints[43]

$$\tilde{u} = U_{\tilde{w}} = c\tilde{x};\ \ \tilde{v} = 0;\ \ \tilde{T} = \tilde{T}_{\tilde{w}};\ \text{at}\ \ \tilde{y} = 0$$

$$\tilde{u} \to 0;\ \tilde{T} \to \tilde{T}_{\infty};\ \text{as}\ \tilde{y} \to \infty \qquad \ldots (4)$$

The thermophysical characteristics and the numerical values for density, thermal expansion coefficient, thermal conductivity, and heat capacity associated with $Cu, Al_2O_3,$ and $TiO_2$ nanoparticles and $H_2O$ are illustrated in Tables 1 and 2.

Following are the similarity variables utilized to non-dimensionalize the PDEs mentioned above[6,35,41]

$$\psi = \tilde{x}\sqrt{c\nu_f}\,f(\eta);\ \tilde{u} = \frac{\partial\psi}{\partial\tilde{y}};\ \tilde{v} = -\frac{\partial\psi}{\partial\tilde{x}};\ \theta(\eta) = \frac{\tilde{T}-\tilde{T}_{\infty}}{\tilde{T}_{\tilde{w}}-\tilde{T}_{\infty}};$$

$$\eta = \sqrt{\frac{c}{\nu_f}}\,\tilde{y} \qquad \ldots (5)$$

The equation of continuity (1) is identically gratified and (2)-(4) takes on the following form

$$g''' - N_1N_2\left(g'^2 - gg''\right) + N_1N_3\lambda\theta = 0 \qquad \ldots (6)$$

$$N_5\theta'' + Rd\,\theta'' + N_4\,\mathrm{Pr}\,g\theta' - \delta_e N_4\,\mathrm{Pr}\left(gg'\theta' + g^2\theta''\right) = 0 \qquad \ldots (7)$$

Table 2 — Numerical values of thermal conductivity, thermal expansion coefficient, heat capacity, and density of the nanoparticles and the base fluid[15,24]

| Thermophysical Characteristics | $Cu$ | $Al_2O_3$ | $TiO_2$ | $H_2O$ |
|---|---|---|---|---|
| $k\left(Wm^{-1}K^{-1}\right)$ | 400 | 40 | 8.9538 | 0.613 |
| $\beta\times10^{-5}\left(K^{-1}\right)$ | 1.67 | 0.85 | 0.9 | 21 |
| $c_p\left(J/kgK\right)$ | 385 | 765 | 686 | 4179 |
| $\rho\left(kgm^{-3}\right)$ | 8933 | 3970 | 4250 | 997.1 |

At $\eta = 0,\quad g = 0,\ g' = 1,\quad \theta = 1$

$$\ldots (8)$$

As $\eta \to \infty$, $g' \to 0,\quad \theta \to 0$

Where $\lambda = \dfrac{Gr_{\tilde{x}}}{\mathrm{Re}_{\tilde{x}}^{\,2}};\quad Gr_{\tilde{x}} = \dfrac{g_r(\beta_T)_f\left(\tilde{T}_{\tilde{w}}-\tilde{T}_{\infty}\right)\tilde{x}^3}{\nu_f^{\,2}};\quad \mathrm{Re}_{\tilde{x}} = \dfrac{\tilde{x}U_{\tilde{w}}}{\nu_f};$

$Rd = \dfrac{16}{3}\dfrac{\sigma^*\tilde{T}_{\infty}^3}{k^*k_f};\quad \mathrm{Pr} = \dfrac{\nu_f}{\alpha_f};\quad \delta_e = c\lambda_\tau$ are the non-dimensional parameters involved in (6)-(7). Also, it should be noted that $\lambda > 0$ indicates aiding flow, $\lambda < 0$ represents impeding flow and $\lambda = 0$ signifies forced convection flow. $N_1,\ N_2,\ N_3,\ N_4$ and $N_5$ are described by,

$$N_1 = \left[(1-\phi_1)(1-\phi_2)(1-\phi_3)\right]^{10/4}$$

$$N_2 = (1-\phi_1)\left(\left(1-\phi_2\right)\left[1-\phi_3+\phi_3\frac{\rho_3}{\rho_f}\right]+\phi_2\frac{\rho_2}{\rho_f}\right)+\phi_1\frac{\rho_1}{\rho_f}$$

$$N_3 = (1-\phi_1)\left(\left(1-\phi_2\right)\left[1-\phi_3+\phi_3\frac{(\rho\beta_T)_3}{(\rho\beta_T)_f}\right]+\phi_2\frac{(\rho\beta_T)_2}{(\rho\beta_T)_f}\right)+\phi_1\frac{(\rho\beta_T)_1}{(\rho\beta_T)_f}$$

$$N_4 = (1-\phi_1)\left(\left(1-\phi_2\right)\left[1-\phi_3+\phi_3\frac{(\rho c_p)_3}{(\rho c_p)_f}\right]+\phi_2\frac{(\rho c_p)_2}{(\rho c_p)_f}\right)+\phi_1\frac{(\rho c_p)_1}{(\rho c_p)_f}$$

$$N_5 = \frac{k_{tnf}}{k_f} = \left(\frac{k_1+2k_{hnf}-2\phi_1\left(k_{hnf}-k_1\right)}{k_1+2k_{hnf}+\phi_1\left(k_{hnf}-k_1\right)}\right)$$
$$\left(\frac{k_2+2k_{nf}-2\phi_2\left(k_{nf}-k_2\right)}{k_2+2k_{nf}+\phi_2\left(k_{nf}-k_2\right)}\right)$$
$$\left(\frac{k_3+2k_f-2\phi_3\left(k_f-k_3\right)}{k_3+2k_f+\phi_3\left(k_f-k_3\right)}\right)$$

The dimensional form of the engineering quantities of interest, skin friction coefficient $\left(C_{f\tilde{x}}\right)$, and Nusselt number $\left(Nu_{\tilde{x}}\right)$ is given by[43]

$$C_{f\tilde{x}} = \frac{\tau_w\left|\tilde{y}=0\right.}{\rho_f\left(\tilde{U}_w\right)^2} \text{ and } Nu_{\tilde{x}} = \frac{\tilde{x}q_w\left|\tilde{y}=0\right.}{k_f\left(\tilde{T}_w-\tilde{T}_\infty\right)} \quad \ldots (9)$$

In which $\tau_w = \mu_{tnf}\dfrac{\partial\tilde{u}}{\partial\tilde{y}}$ describes the shear stress and $q_w = -k_{tnf}\dfrac{\partial\tilde{T}}{\partial\tilde{y}} - \dfrac{16}{3}\dfrac{\sigma^*\tilde{T}_\infty^3}{k^*}\dfrac{\partial\tilde{T}}{\partial\tilde{y}}$ is the heat flux.

(9) takes the following dimensionless form by making use of the similarity transformation (5),

$$C_{f\tilde{x}}\,\mathrm{Re}_{\tilde{x}}^{1/2} = \frac{1}{N_1}f''(0),\ Nu_{\tilde{x}}\,\mathrm{Re}_{\tilde{x}}^{-1/2} = -\left(N_5+Rd\right)\theta'(0) \quad \ldots (10)$$

**Numerical Solution**

The system of non-linear differential equations (6)-(7) is initially transformed into a system of first order ODEs by implementing the following procedure.

$$g = m_1,\ \ g' = m_2,\ \ g'' = m_3,\ \ \theta = m_4,\ \ \theta' = m_5, \quad \ldots (11)$$

Invoking (11) in (6) and (7), we obtain,

$$m_3' = g''' = N_1N_2\left(m_2^2-m_1m_3\right)-N_1N_3\lambda m_4$$

$$m_5' = \theta'' = \frac{1}{\left(N_5+Rd-m_1^2\delta_eN_4\,\mathrm{Pr}\right)}$$
$$\left[\delta_eN_4\,\mathrm{Pr}\,m_1m_2m_5 - N_4\,\mathrm{Pr}\,m_1m_5\right]$$

The corresponding transmuted boundary conditions are,

$$m_1 = 0,\ \ m_2 = 1,\ \ m_4 = 1,\ \text{ at }\ \eta = 0$$

$$m_2 \to 0,\ \ m_4 \to 0 \ \text{ as } \ \eta \to \infty$$

The remodelled ODEs are evaluated numerically with the bvp4c function in MATLAB software. Depending on the values of the parameters that were used, we selected $\eta \to \infty$ values to be 5 (i.e.) $\eta_\infty = 5$.

**Results and Discussion**

A graphical interpretation of the effects of numerous dimensionless, pertinent parameters on the ternary hybrid nanofluid flow profiles is discussed in the current section. These parameters include mixed convection parameter $\lambda$, Prandtl number $\mathrm{Pr}$, thermal relaxation parameter $\delta_e$, radiation parameter $Rd$, and volume fraction $\phi$. Here, $\phi_1, \phi_2, \phi_3$ respectively denotes the volume fraction of $Cu, Al_2O_3$, and $TiO_2$ nanoparticles. The established Prandtl number for water is approximately 6.9 and hence our investigation strategically encompasses a range of Prandtl numbers, specifically targeting values between 6 and 6.9 $\left(6\cdot0 \le \mathrm{Pr} \le 6.9\right)$. Since the Brinkman viscosity model has been employed, the volume fraction of nanoparticles has been constrained to be less than 4% $\left(0\cdot01 \le \phi < 0.04\right)$. The mixed convection parameter is deliberately set between -1 and 2 to examine the effects of assisting, opposing, and forced convective flows on the flow profiles $\left(-1 \le \lambda \le 2\right)$. Also, the thermal relaxation parameter and radiation parameter are set within the range $\left(0\cdot01 \le \delta_e \le 0\cdot2\right)$ and $\left(0\cdot1 \le Rd \le 2.5\right)$ following[32,29,41].

**Scrutinization of velocity field**

Influence of buoyancy parameter on the velocity field for $Cu/H_2O$ nanofluid, $Cu-Al_2O_3/H_2O$ hybrid nanofluid and $Cu-Al_2O_3-TiO_2/H_2O$ ternary hybrid nanofluid is presented in Fig. 2. Accelerating the buoyancy parameter results in an enhancement of the velocity profile. Mixed convection, in general, is described by the buoyancy force versus the inertial force ratio. As $\lambda$ enhances, the influence of buoyancy forces becomes dominant over the inertial forces, thereby boosting the velocity.

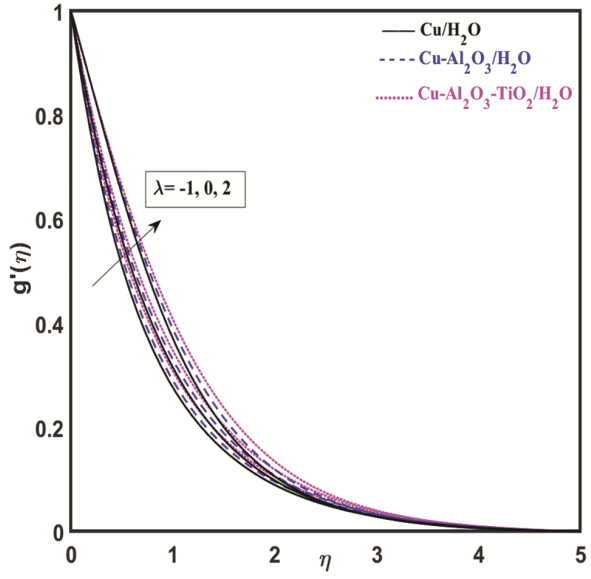


Fig. 2 — Implication of $\lambda$ on $g'(\eta)$

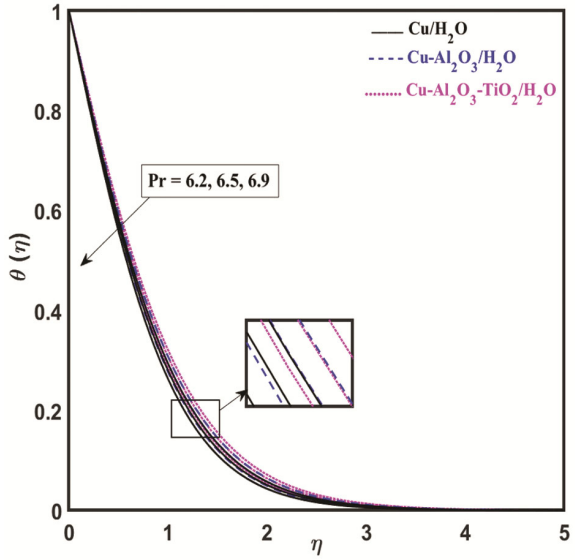


Fig. 3 — Implication of Pr on $\theta(\eta)$

**Scrutinization of temperature field**

Fig. 3 depicts the variation in temperature against different values of Pr for $Cu/H_2O$ nanofluid, $Cu-Al_2O_3/H_2O$ hybrid nanofluid and $Cu-Al_2O_3-TiO_2/H_2O$ ternary hybrid nanofluid. It is observed that maximizing the Pr values decline the thermal profile. The Prandtl number relates inversely to heat diffusivity by definition. An augmentation in the Pr values diminishes the heat diffusion rate and hence the temperature of the liquid reduces. A demonstration of how the thermal field is affected by radiation parameter $Rd$ is portrayed in Fig. 4. A rise in temperature is perceived with expanding values of radiation parameter $Rd$. Fig. 5 represents the sway of thermal relaxation parameter $\delta_e$ on the thermal gradient for $Cu/H_2O$ nanofluid, $Cu-Al_2O_3/H_2O$ hybrid and $Cu-Al_2O_3-TiO_2/H_2O$ tri-hybrid nanofluid. Accelerating the $\delta_e$ values constrict the temperature sketch of nanofluid, hybrid and ternary hybrid nanofluid. The conductive behavior of the fluid particles decreases with proliferating $\delta_e$ values, thus leading to a depletion in temperature.

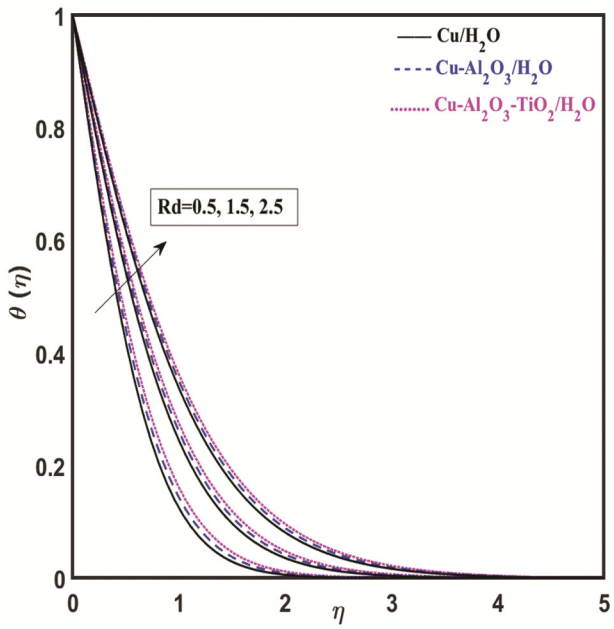


Fig. 4 — Implication of $Rd$ on $\theta(\eta)$

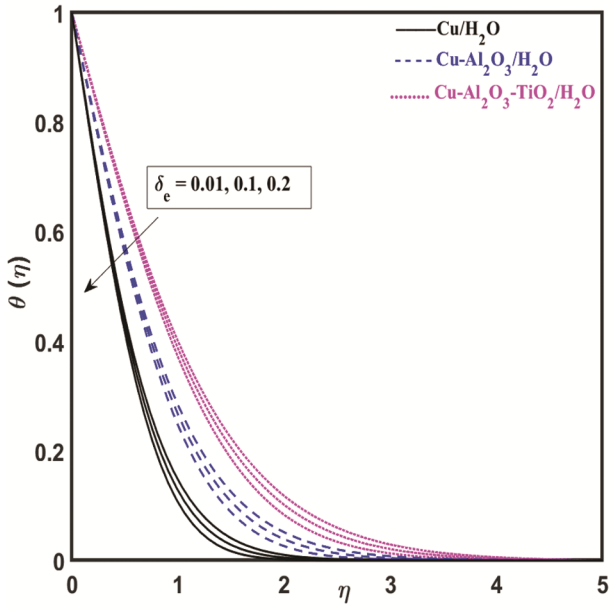


Fig. 5 — Implication of $\delta_e$ on $\theta(\eta)$

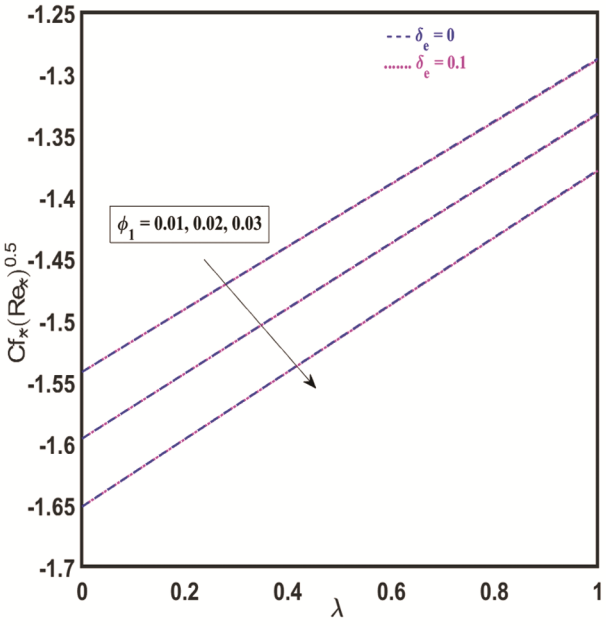


Fig. 6 — Implication of $\phi_1$ and $\lambda$ on $C_{f\tilde{x}}\left(\mathrm{Re}_{\tilde{x}}\right)^{0.5}$

**Scrutinization of engineering quantities of interest**

Fig. 6 illustrates the discrepancy in the values of skin-friction coefficient against $\lambda$ for distinct values of $\phi_1$. It can be inferred from the figure that the graph of $C_{f\tilde{x}}\left(\mathrm{Re}_{\tilde{x}}\right)^{0.5}$ gets compressed with an enhancement in the values of $\phi_1$ but intensifies through $\lambda$. Also,

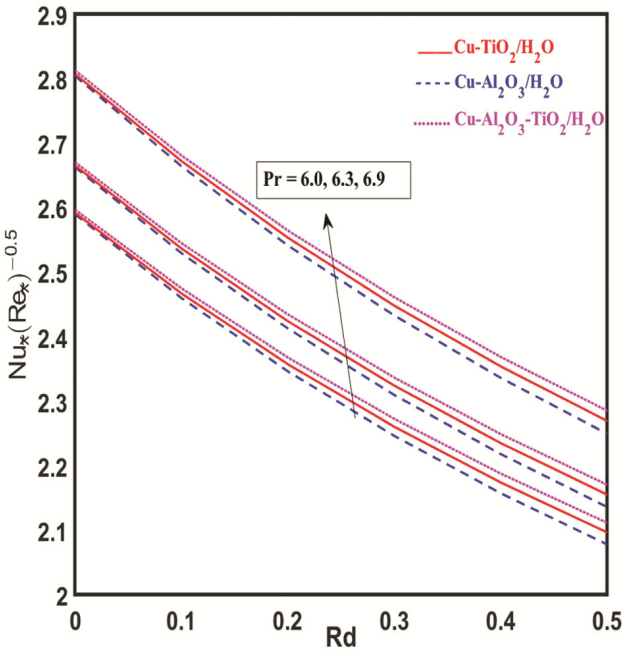


Fig. 7 — Implication of Pr and $Rd$ on $Nu_{\tilde{x}}\left(\mathrm{Re}_{\tilde{x}}\right)^{-0.5}$

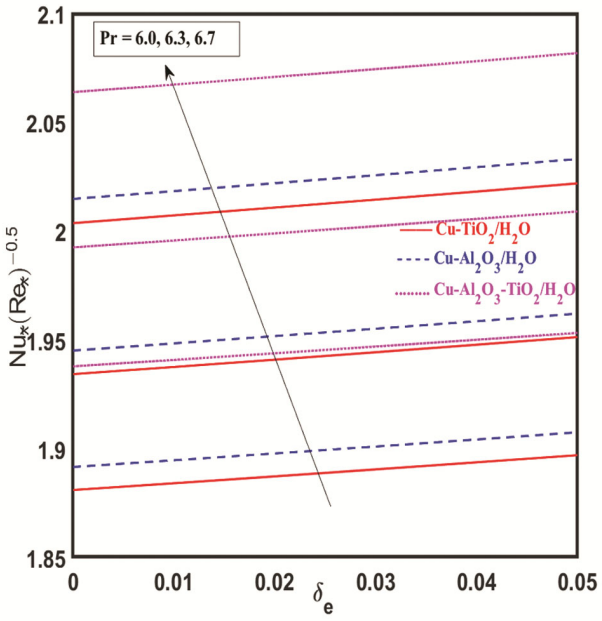


Fig. 8 — Implication of Pr and $\delta_e$ on $Nu_{\tilde{x}}\left(\mathrm{Re}_{\tilde{x}}\right)^{-0.5}$

the values of the drag force seem to be dominating in the absence of $\delta_e$ rather than in the presence of it. The RHT, which is calculated by using Nusselt number, are portrayed in Fig. 7 and 8. According to Fig. 7, the values of $Nu_{\tilde{x}}\left(\mathrm{Re}_{\tilde{x}}\right)^{-0.5}$ increases with Pr

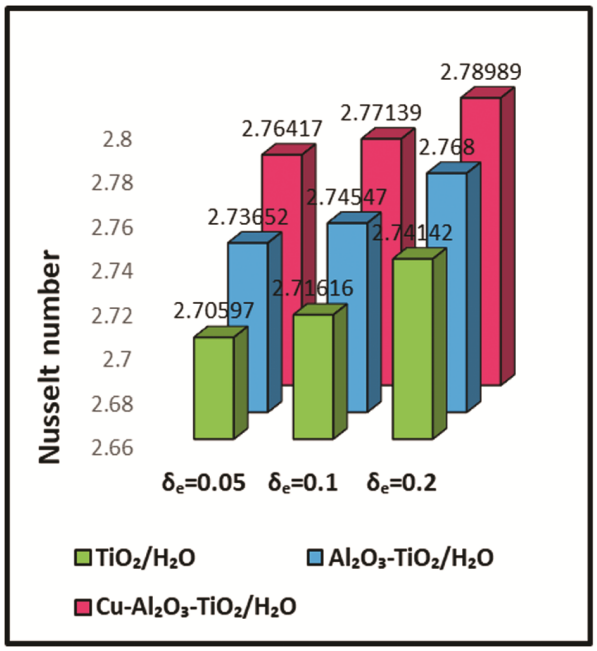


Fig. 9 — Discrepancy in Nusselt number against $\delta_e$

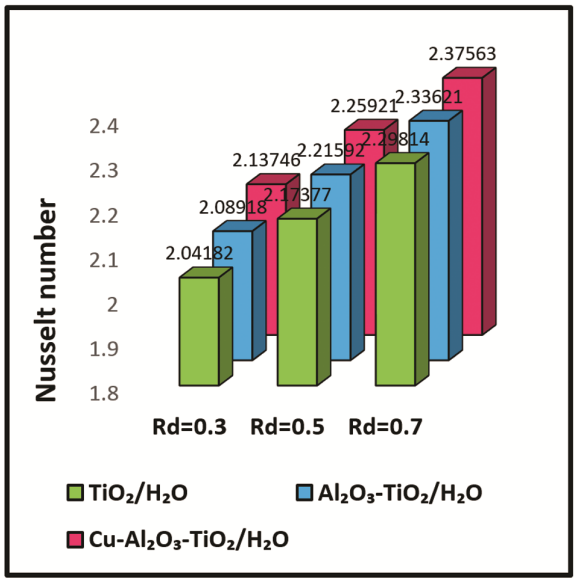


Fig. 10 — Discrepancy in Nusselt number against $Rd$

for the cases of $Cu-TiO_2/H_2O$, $Cu-Al_2O_3/H_2O$ hybrid nanofluid and $Cu-Al_2O_3-\mathrm{TiO}_2/H_2O$ ternary nanofluid. The sway of Prandtl number Pr and thermal relaxation parameter $\delta_e$ on $Nu_{\bar{x}}\left(\mathrm{Re}_{\bar{x}}\right)^{-0.5}$ is displayed in Fig. 8. It is visualised that the RHT intensifies for improved values of Pr and $\delta_e$. Also, the trihybrid nanofluid

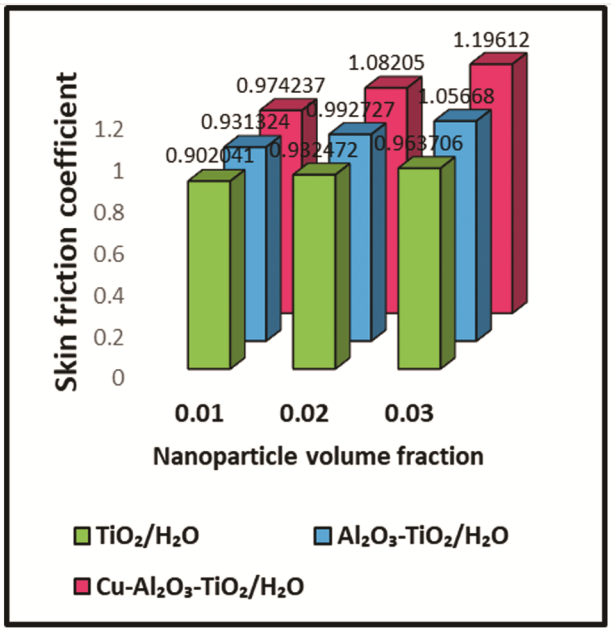


Fig. 11 — Skin friction analysis of ternary hybrid nanofluid based on $\phi_1, \phi_2$, and $\phi_3$

$Cu-Al_2O_3-\mathrm{TiO}_2/H_2O$ appears to have significantly higher RHT than $Cu-TiO_2/H_2O$ and $Cu-Al_2O_3/H_2O$ hybrid nanofluid.

The influence of thermal relaxation parameter $\delta_e$ and radiation parameter $Rd$ on the RHT for $\mathrm{TiO}_2/H_2O$ nanofluid, $Al_2O_3-\mathrm{TiO}_2/H_2O$ hybrid nanofluid and $Cu-Al_2O_3-\mathrm{TiO}_2/H_2O$ ternary hybrid nanofluid are illustrated in Figs 9-10. The RHT for $\mathrm{TiO}_2/H_2O$ nanofluid upsurges from 2.70597 to 2.74142 when $\delta_e$ varies between 0.05 and 0.2. During the same range of $\delta_e$, $Al_2O_3-\mathrm{TiO}_2/H_2O$ hybrid nanofluid and $Cu-Al_2O_3-\mathrm{TiO}_2/H_2O$ ternary hybrid nanofluid exhibit thermal transmission rates ranging from 2.73652 to 2.768 and 2.76417 to 2.78989, respectively. Additionally, the ternary hybrid nanofluid demonstrated better rate of thermal transfer compared to $\mathrm{TiO}_2/H_2O$ hybrid nanofluid by approximately 3.26-4.47 % for varying values of radiation parameter. Thus, augmenting the values of $\delta_e$ and $Rd$ seems to have a positive impact on the thermal transfer rate.

Fig. 11-12 illustrate the variation in surface drag force and thermal transfer coefficient with a greater

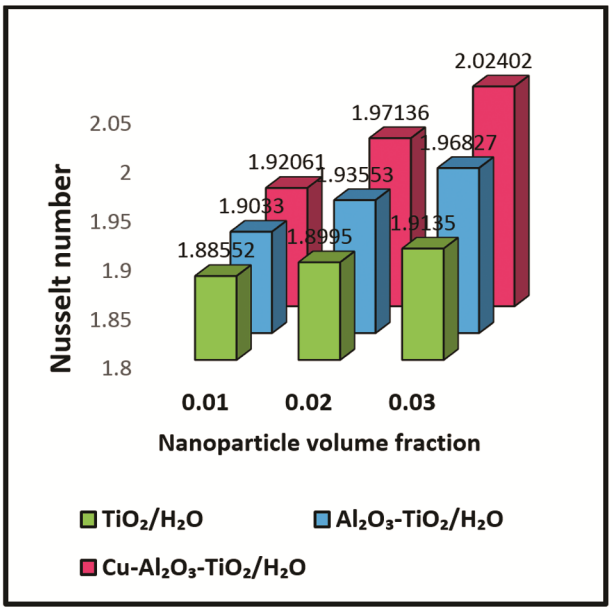


Fig. 12 — Nusselt number analysis of ternary hybrid nanofluid based on $\phi_1, \phi_2$, and $\phi_3$

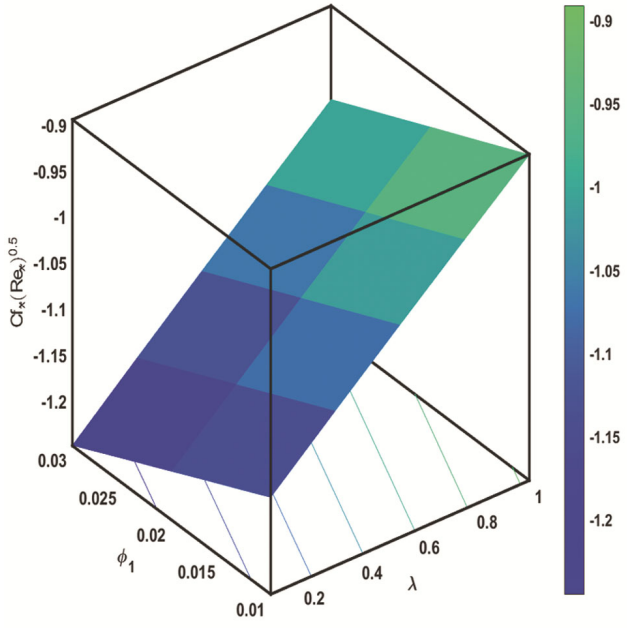


Fig. 13 — Implication of $\lambda$ and $\phi_1$ on $C_{f\tilde{x}}\left(\mathrm{Re}_{\tilde{x}}\right)^{0.5}$

fraction of the nanoparticles, $\phi_1, \phi_2$, and $\phi_3$. As a result of variations in $\phi_1, \phi_2$, and $\phi_3$ values between 0.01 and 0.03, the skin friction coefficients of $\mathrm{TiO_2}/H_2O$ nanofluid vary from 0.902041 to

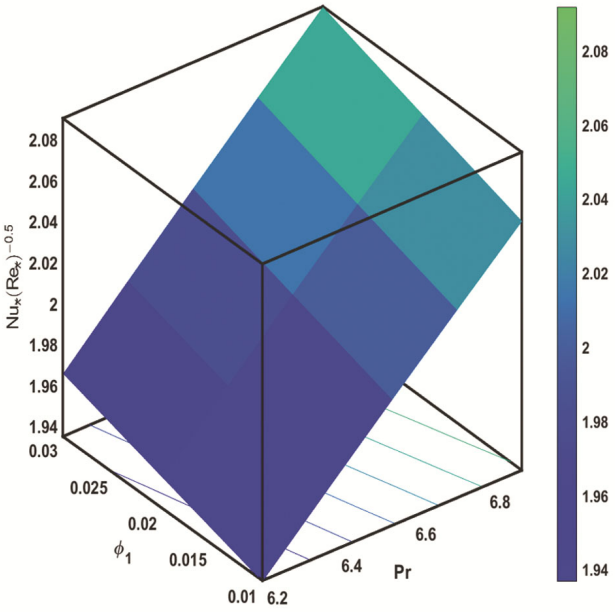


Fig. 14 — Implication of $\mathrm{Pr}$ and $\phi_1$ on $Nu_{\tilde{x}}\left(\mathrm{Re}_{\tilde{x}}\right)^{-0.5}$

0.963706 and for $Al_2O_3-\mathrm{TiO_2}/H_2O$ hybrid nanofluid, they range from 0.931324 to 1.05668 whereas for $Cu-Al_2O_3-\mathrm{TiO_2}/H_2O$, the surface drag force vary between 0.974237 to 1.19612. It can be inferred from Fig. 12 that the thermal transfer of $Cu-Al_2O_3-\mathrm{TiO_2}/H_2O$ enhances by 1.83-5.46% approximately when compared to $\mathrm{TiO_2}/H_2O$ when $\phi_1, \phi_2$, and $\phi_3$ varies from 0.01 to 0.03. Thus, boosting the volume fraction accelerates the RHT of $Cu-Al_2O_3-\mathrm{TiO_2}/H_2O$. The purpose of Fig. 13 is to examine how $\lambda$ and $\phi_1$ influence $C_{f\tilde{x}}\left(\mathrm{Re}_{\tilde{x}}\right)^{0.5}$. Here $C_{f\tilde{x}}\left(\mathrm{Re}_{\tilde{x}}\right)^{0.5}$ upsurges for higher $\lambda$ while it diminishes for enhancing $\phi_1$ values. Fig. 14 exhibits that $Nu_{\tilde{x}}\left(\mathrm{Re}_{\tilde{x}}\right)^{-0.5}$ gets positively influenced by the increasing $\mathrm{Pr}$ and $\phi_1$ values. The performance of $Nu_{\tilde{x}}\left(\mathrm{Re}_{\tilde{x}}\right)^{-0.5}$ with reference to $Rd$ and $\delta_e$ is depicted in Fig. 15. It is perceived that $Nu_{\tilde{x}}\left(\mathrm{Re}_{\tilde{x}}\right)^{-0.5}$ augments with both elevating $Rd$ and $\delta_e$ values. The variation of the streamline patterns on the $Cu-Al_2O_3-\mathrm{TiO_2}/H_2O$ flow with respect to the

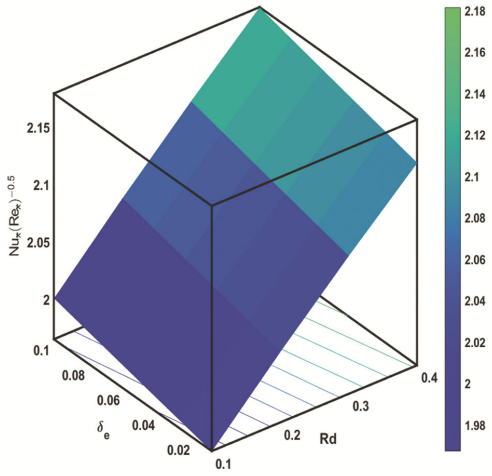


Fig. 15 — Implication of $Rd$ and $\delta_e$ on $Nu_{\tilde{x}}\left(\mathrm{Re}_{\tilde{x}}\right)^{-0.5}$

mixed convection parameter $\lambda$ is elucidated through Fig. 16(a-b). Essentially, a consistently augmented $\lambda$ produces a considerable buoyant force resulting in more kinetic energy which in turn boosts the velocity profile of $Cu-Al_2O_3-\mathrm{TiO}_2/H_2O$. The features of $Nu_{\tilde{x}}\left(\mathrm{Re}_{\tilde{x}}\right)^{-0.5}$ for various parameters are detailed in Table 3. The heat transmission coefficient $Nu_{\tilde{x}}\left(\mathrm{Re}_{\tilde{x}}\right)^{-0.5}$ enhances for increasing $Rd$, Pr and $\delta_e$ values.

**Affirmation of results**

The accuracy of the obtained results is evaluated in Table 4. The current results are validated for a special case of our work by those earlier reported results[42-45]. It is evident that there is an exceptional agreement between the outcomes.

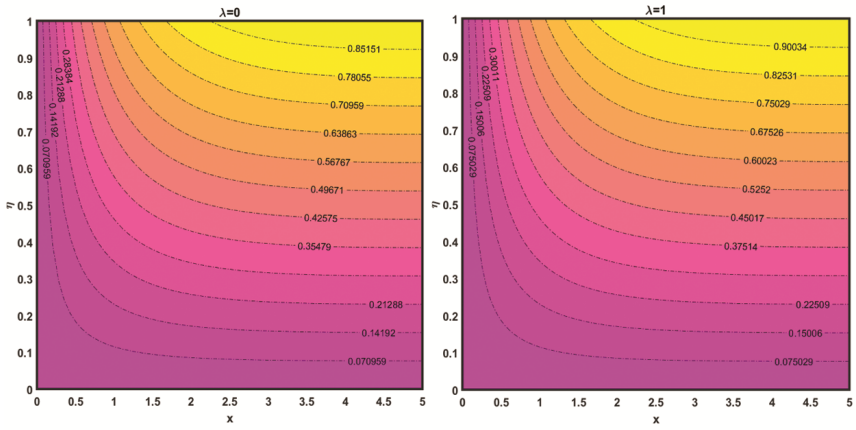


Fig.16 — Streamlines for $Cu-Al_2O_3-\mathrm{TiO}_2/H_2O$ for (a) $\lambda=0$ (b) $\lambda=1$

Table 3 — Numerical results of $Nu_{\tilde{x}}\left(\mathrm{Re}_{\tilde{x}}\right)^{-0.5}$ with regard to distinct parameters

| $\lambda$ | $Rd$ | Pr | $\delta_e$ | $Nu_{\tilde{x}}\left(\mathrm{Re}_{\tilde{x}}\right)^{-0.5}$ |
|---|---|---|---|---|
| 0.1 | 0.1 | 6.2 | 0.02 | 2.40945 |
| | 0.2 | | | 2.62314 |
| | 0.3 | | | 2.85482 |
| 0.1 | 0.4 | 6.2 | 0.02 | 3.10729 |
| | | 6.5 | | 3.19416 |
| | | 6.9 | | 3.30696 |
| 0.1 | 0.4 | 6.2 | 0.01 | 3.1013 |
| | | | 0.03 | 3.11331 |
| | | | 0.05 | 3.12544 |

Table 4 — Comparison of $-\theta'(0)$ with[42-45] when $\phi_1=\phi_2=\phi_3=Rd=\delta_e=\lambda=0$

| Pr | Ahmad *et al.*[42] | Khan *et al.*[43] | Shaiq *et al.*[44] | Devi and Devi[45] | Current results |
|---|---|---|---|---|---|
| 2 | 0.9111 | 0.9119 | 0.9114 | 0.91135 | 0.9112395 |
| 6.13 | 1.7595 | - | - | 1.75968 | 1.7596364 |
| 7.0 | 1.8952 | 1.8994 | 1.8954 | 1.89540 | 1.8953462 |
| 20.0 | 3.3538 | 3.3533 | 3.3539 | 3.35390 | 3.3539254 |

## Conclusion

The current study examines the mixed convective flow of a $Cu-Al_2O_3-\mathrm{TiO}_2/H_2O$ ternary hybrid nanofluid past an elongated sheet with the application of C-C heat flux model. Additionally, the sway of heat radiation is also considered. By utilizing the similarity transformation, the equations governing the flow were transformed into dimensionless ODEs, which were followed by a numerical solution. The results listed below are some of the substantial conclusions made from this investigation:

- The augmentation of mixed convective parameter leads to an enhancement in the velocity profile.
- Increasing the radiation parameter enhances the temperature profile of the tri-hybrid nanofluid.
- The skin friction coefficient of $Cu-Al_2O_3-\mathrm{TiO}_2/H_2O$ surpasses $Al_2O_3-\mathrm{TiO}_2/H_2O$ approximately by 4.4-11.7% for varying volume fraction of the nanoparticles.
- An elevation in thermal relaxation parameter strongly boosts the rate of heat transfer.
- The tri-hybrid nanofluid $Cu-Al_2O_3-TiO_2/H_2O$ exhibits approximately 1.82-5.46% enhanced thermal transfer efficiency compared to $TiO_2/H_2O$ for increasing values of volume fraction of the nanoparticle.

## Nomenclature

$(\tilde{u},\tilde{v})$ Velocity components along $(\tilde{x},\tilde{y})$ axis

$g_r$ acceleration due to gravity

$\tilde{T}$ Nanofluid temperature

$\tilde{T}_\infty$ Ambient temperature

$\tilde{T}_{\tilde{w}}$ Wall temperature

$k^*$ Mean absorption coefficient

$\lambda$ Mixed convection or buoyancy parameter

$Rd$ Radiation parameter

Pr Prandtl number

$\lambda_\tau$ Thermal relaxation time

$\delta_e$ Thermal relaxation parameter

$\phi_1$ Volume fraction of $Cu$ nanoparticles

$\phi_2$ Volume fraction of $Al_2O_3$ nanoparticles

$\phi_3$ Volume fraction of $TiO_2$ nanoparticles

$\eta$ Similarity variable

$\theta$ non-dimensional temperature

$\mu_f$ Dynamic viscosity of the fluid

$\rho_f$ Density of the fluid

$Gr_{\tilde{x}}$ Local Grashof number

$\mathrm{Re}_{\tilde{x}}$ Local Reynolds number

$c_p$ Specific heat at constant pressure

*Greek symbols*

$\mu_{tnf}$ Viscosity of ternary nanofluid

$\rho_{tnf}$ Density of ternary nanofluid

$(\rho\beta_T)_{tnf}$ Thermal expansion coefficient of ternary nanofluid

$k_{tnf}$ Thermal conductivity of ternary nanofluid

$(\rho c_p)_{tnf}$ Heat capacity of ternary nanofluid

$\sigma^*$ Stefan-Boltzmann constant

$(\rho c_p)_f$ Heat capacity of the fluid

$(\rho\beta_T)_f$ Thermal expansion coefficient of the fluid

$k$ Thermal conductivity of the fluid

*Subscripts*

$f$ fluid

$nf$ nanofluid

$hnf$ hybrid nanofluid

$tnf$ ternary hybrid nanofluid

*Superscript*

$'$ Differentiation with respect to $\eta$

## References


1 Choi S U S & Eastman J A, Enhancing thermal conductivity of fluids with nanoparticles (Argonne National Lab, United States), (1995).

2 Taylor R, Coulombe S, Otanicar T, Phelan P, Gunawan A, Lv W, Rosengarten G, Prasher R & Tyagi H, Small particles, big impacts: A review of the diverse applications of nanofluids, *J Appl Phys*, 113 (2013) 011301.

3 Aparna Z, Michael M, Pabi S K & Ghosh S, Thermal conductivity of aqueous $Al_2O_3$/Ag hybrid nanofluid at different temperatures and volume concentrations: An experimental investigation and development of new correlation function, *Powder Technol*, 343 (2019) 714.

4 Bhattad A & Sarkar J, Effects of nanoparticle shape and size on the thermohydraulic performance of plate evaporator using hybrid nanofluids, *J Therm Anal Calorim*, 143 (2021) 767.

5 Kulkarni M, Mixed convective magnetized GO-MoS2/H2O hybrid nanofluid flow about a permeable rotating disk, *Asia-Pac J Chem Eng*, 18 (2023) e2923.

6 Manjunatha S, Puneeth V, Gireesha B J & Chamkha A, Theoretical Study of Convective Heat Transfer in Ternary Nanofluid Flowing past a Stretching Sheet, *J Appl Comput Mech*, 8 (2022) 1279.

7 Dezfulizadeh A, Aghaei A, Joshaghani A H & Najafizadeh M M, An experimental study on dynamic viscosity and thermal conductivity of water-Cu-$SiO_2$-MWCNT ternary hybrid nanofluid and the development of practical correlations, *Powder Technol*, 389 (2021) 215.

8 Mousavi S M, Esmaeilzadeh F & Wang X P, Effects of temperature and particles volume concentration on the thermophysical properties and the rheological behavior of CuO/MgO/$TiO_2$ aqueous ternary hybrid nanofluid, *J Therm Anal Calorim*, 137 (2019) 879.

9 Sahoo R R, Effect of various shape and nanoparticle concentration based ternary hybrid nanofluid coolant on the thermal performance for automotive radiator, *Heat Mass Transf*, 57 (2021) 873.

10 Adun H, Mukhtar M, Adedeji M, Agwa T, Ibrahim K H, Bamisile O & Dagbasi M, Synthesis and application of ternary nanofluid for photovoltaic-thermal system: Comparative analysis of energy and exergy performance with single and hybrid nanofluids, *Energies*, 14 (2021) 4434.

11 Kashyap S, Sarkar J & Kumar A, Performance enhancement of regenerative evaporative cooler by surface alterations and using ternary hybrid nanofluids, *Energy*, 225 (2021) 120199.

12 Adun H, Kavaz D, Dagbasi M, Umar H & Wole-Osho I, An experimental investigation of thermal conductivity and dynamic viscosity of $Al_2O_3$-ZnO-$Fe_3O_4$ ternary hybrid nanofluid and development of machine learning model, *Powder Technol*, 394 (2021) 1121.

13 Boroomandpour A, Toghraie D & Hashemian M, A comprehensive experimental investigation of thermal conductivity of a ternary hybrid nanofluid containing MWCNTs- titania-zinc oxide/water-ethylene glycol (80:20) as well as binary and mono nanofluids, *Synth Met*, 268 (2020) 116501.

14 Ahmed W, Kazi S N, Chowdhury Z Z, Johan M R B, Mehmood S, Soudagar M E M, Mujtaba M A, Gul M & Ahmad M S, Heat transfer growth of sonochemically synthesized novel mixed metal oxide ZnO+$Al_2O_3$+$TiO_2$/DW based ternary hybrid nanofluids in a square flow conduit, *Renew Sust Energ Rev*, 145 (2021) 111025.

15 Puneeth V, Anandika R, Manjunatha S, Khan M I, Khan M I, Althobaiti A & Galal A M, Implementation of modified Buongiorno's model for the investigation of chemically reacting rGO-$Fe_3O_4$-$TiO_2$-$H_2O$ ternary nanofluid jet flow in the presence of bio-active mixers, *Chem Phys Lett*, 786 (2022) 139194.

16 Sahoo R R, Heat transfer and second law characteristics of radiator with dissimilar shape nanoparticle-based ternary hybrid nanofluid, *J Therm Anal Calorim*, 146 (2021) 827.

17 El-Shorbagy M A, Eslami F, Ibrahim M, Barnoon P, Xia W & Toghraie D, Numerical investigation of mixed convection of nanofluid flow in a trapezoidal channel with different aspect ratios in the presence of porous medium, *Case Stud Therm Eng*, 25 (2021) 100977.

18 Al-Farhany K & Abdulsahib A D, Study of mixed convection in two layers of saturated porous medium and nanofluid with rotating circular cylinder, *Prog Nucl Energy*, 135 (2021) 103723.

19 Waini I, Ishak A, Groşan T & Pop I, Mixed convection of a hybrid nanofluid flow along a vertical surface embedded in a porous medium, *Int Commun Heat Mass Transf*, 114 (2020) 104565.

20 Boumaiza N, Kezzar M, Eid M R & Tabet I, On numerical and analytical solutions for mixed convection Falkner-Skan flow of nanofluids with variable thermal conductivity, *Waves Random Complex Media*, 31 (2021) 1550.

21 Mishra A, Priyadarsan K P, Mishra S & Nayak M K, MHD nonlinear radiative flow of Carreau nanofluid with variable chemical reaction: An approach to control global warming, *Heat Transf*, 50 (2021) 542.

22 Sheikholeslami M, Numerical investigation of nanofluid free convection under the influence of electric field in a porous enclosure, *J Mol Liq*, 249 (2018) 1212.

23 Yashkun U, Zaimi K, Ishak A, Pop I & Sidaoui R, Hybrid nanofluid flow through an exponentially stretching/shrinking sheet with mixed convection and Joule heating, *Int J Numer Method Heat Fluid Flow*, 31 (2021) 1930.

24 Waini I, Ishak A & Pop I, Mixed convection flow over an exponentially stretching/shrinking vertical surface in a hybrid nanofluid, *Alex Eng J*, 59 (2020) 1881.

25 Ghosh S & Mukhopadhyay S, Unsteady mixed convective flow of nanofluid with arbitrary-shaped nanoparticles over a shrinking sheet, *Asia-Pac J Chem Eng*, 16 (2021) e2624.

26 Pordanjani A H, Aghakhani S, Karimipour A, Afrand M & Goodarzi M, Investigation of free convection heat transfer and entropy generation of nanofluid flow inside a cavity affected by magnetic field and thermal radiation, *J Therm Anal Calorim*, 137 (2019) 997.

27 Reddy P S & Sreedevi P, Effect of thermal radiation and volume fraction on carbon nanotubes based nanofluid flow inside a square chamber, *Alex Eng J*, 60 (2021) 1807.

28 Jamshed W, Devi S U S, Goodarzi M, Prakash M, Nisar K S, Zakarya M & Abdel-Aty A, Evaluating the unsteady Casson nanofluid over a stretching sheet with solar thermal radiation: An optimal case study, *Case Stud Therm Eng*, 26 (2021) 101160.

29 Sreedevi P, Reddy P S & Chamkha A, Heat and mass transfer analysis of unsteady hybrid nanofluid flow over a stretching sheet with thermal radiation, *SN Appl Sci*, 2 (2020) 1222.

30 Wahid N S, Md Arifin N, Khashi'ie N S, Pop I, Bachok N & Hafidzuddin M E H, MHD mixed convection flow of a hybrid nanofluid past a permeable vertical flat plate with thermal radiation effect, *Alex Eng J*, 61 (2022) 3323.

31 Reddy P S, Sreedevi P & Chamkha A J, Heat and mass transfer analysis of nanofluid flow over swirling cylinder with Cattaneo–Christov heat flux, *J Therm Anal Calorim*, 147 (2022) 3453.

32 Abid N, Ramzan M, Chung J D, Kadry S & Chu Y, Comparative analysis of magnetized partially ionized copper, copper oxide–water and kerosene oil nanofluid flow with Cattaneo–Christov heat flux, *Sci Rep*, 10 (2020) 19300.

33 Azam M, Effects of Cattaneo-Christov heat flux and nonlinear thermal radiation on MHD Maxwell nanofluid with Arrhenius activation energy, *Case Stud Therm Eng*, 34 (2022) 102048.

34 Khan M J, Duraisamy B, Zuhra S, Nawaz R, Nisar K S, Jamshed W & Yahia I S, Numerical solution of Catteno-Christov heat flux model over stretching/shrinking hybrid nanofluid by new iterative method, *Case Stud Therm Eng*, 28 (2021) 101673.

35 Waqas H, Farooq U, Liu D, Imran M, Muhammad T, Alshomrani A S & Umar M, Comparative analysis of hybrid nanofluids with Cattaneo-Christov heat flux model: A thermal case study, *Case Stud Therm Eng*, 36 (2022) 102212.

36 Shaw S, Impact of Cattaneo–Christov Heat Flux On $Al_2O_3$–Cu/$H_2O$–$(CH_2OH)_2$ Hybrid Nanofluid Flow Between Two Stretchable Rotating Disks, *Energ Syst Nanotechnol*, (2021) 329.

37 Reddy P S, Sreedevi P & Venkateswarlu S, Impact of modified Fourier's heat flux on the heat transfer of MgO/$Fe_3O_4$–Eg-based hybrid nanofluid flow inside a square chamber, *Waves Random Complex Media*, (2022) 1.

38 Muhammad N, Nadeem S, Khan U, Sherif E M & Issakhov A, Insight into the significance of Richardson number on two-phase flow of ethylene glycol-silver nanofluid due to Cattaneo-Christov heat flux, *Waves Random Complex Media*, (2021) 1.

39 Khan S U, Irfan M, Khan M I, Abbasi A, Rahman S U, Niazi U M & Farooq S, Bio-convective Darcy-Forchheimer oscillating thermal flow of Eyring-Powell nanofluid subject to exponential heat source/sink and modified Cattaneo–Christov model applications, *J Indian Chem Soc*, 99 (2022) 100399.

40 Rana S, Mehmood R & Muhammad T, On homogeneous-heterogeneous reaction in oblique stagnation-point flow of Jeffery liquid involving Cattaneo-Christov heat flux, *Therm Sci*, 25 (2021) 165.

41 Venkateswarlu B & Satya Narayana P V, Cu-$Al_2O_3$/$H_2O$ hybrid nanofluid flow past a porous stretching sheet due to temperatue-dependent viscosity and viscous dissipation, *Heat Transf*, 50 (2021) 432.

42 Ahmad F, Abdal S, Ayed H, Hussain S, Salim S & Almatroud A O, The improved thermal efficiency of Maxwell hybrid nanofluid comprising of graphene oxide plus silver / kerosene oil over stretching sheet, *Case Stud Therm Eng*, 27 (2021) 101257.

43 Khan S A, Khan M I, Hayat T & Alsaedi A, Darcy-Forchheimer hybrid ($MoS_2$, $SiO_2$) nanofluid flow with entropy generation, *Comput Meth Prog Bio*, 185 (2020) 105152.

44 Shaiq S, Maraj E N & Iqbal Z, Remarkable role of $C_3H_8O_2$ on transportation of $M_oS_2$-$S_iO_2$ hybrid nanoparticles influenced by thermal deposition and internal heat generation, *J Phys Chem Solids*, 126 (2019) 294.

45 Devi S U S & Devi S P A, Heat transfer enhancement of $C_u$ – $A_{l2}O_3$/*Water* hybrid nanofluid flow over a stretching sheet, *J Niger Math Soc*, 36 (2017) 419.